

Observation of Magnetocoriolis Waves in a Liquid Metal Taylor-Couette Experiment

M. D. Nornberg,* H. Ji, E. Schartman, A. Roach, and J. Goodman

*Center for Magnetic Self Organization in Laboratory and Astrophysical Plasmas and Princeton Plasma Physics Laboratory,
P.O. Box 451 Princeton, New Jersey 08543, USA*

(Received 2 September 2009; published 18 February 2010)

The first observation of fast and slow magnetocoriolis (MC) waves in a laboratory experiment is reported. Rotating nonaxisymmetric modes arising from a magnetized turbulent Taylor-Couette flow of liquid metal are identified as the fast and slow MC waves by the dependence of the rotation frequency on the applied field strength. The observed slow MC wave is damped but the observation provides a means for predicting the onset of the magnetorotational instability.

DOI: 10.1103/PhysRevLett.104.074501

PACS numbers: 47.65.Cb, 52.35.Bj, 94.30.cq

Hydromagnetic waves are a ubiquitous feature of both geophysical and solar dynamo models as well as models of astrophysical accretion disks. Such waves were first observed in experiments [1] with liquid metals using a sufficiently strong magnetic field that the Lorentz force could act like tension on a string and support Alfvén waves [2]. When the liquid is in rapid rotation, these waves are modified by the Coriolis force. The resultant magnetocoriolis waves [3] are a hybrid of Alfvén waves and inertial waves [4]. Magnetocoriolis waves (MC waves) are used to explain the secular variation of Earth's magnetic field over the course of hundreds of years [5] and the redistribution of angular momentum in the Sun [6]. They are a special case of the more general magnetic archimedes coriolis (MAC) waves from dynamo theory [7,8].

Despite the importance of MC waves in rotating conducting fluids and plasmas there is scant experimental evidence of their existence and of their relationship to various important astrophysical phenomena such as the dynamo or the magnetorotational instability (MRI) [9–11]. Recent experiments [12] on a liquid sodium spherical Couette device and simulations [13] have found several different types of hydromagnetic waves, but there is ambiguity about their identification as MC waves. A similar experiment in Maryland found inertial waves [14], but the applied fields were too weak to observe Lorentz force effects.

In this Letter, we report the first clear identification of the combined fast and slow MC waves in a laboratory experiment. Through measurements of the radial magnetic field in a liquid metal Taylor-Couette flow, we observe two rotating modes that follow the rotation speeds expected for the fast and slow MC wave. We also demonstrate through a local stability analysis that with the addition of sufficient flow shear, the slow MC wave can be destabilized to produce the MRI. Using the observed frequencies of the waves we infer from the local dispersion relation that the modes are damped and obtain a method of determining the threshold for the MRI.

The Princeton MRI experiment is designed to study the stability of a rotating sheared flow of liquid metal with an

applied magnetic field coaxial with the rotation axis. The apparatus has been described elsewhere [15] and has already demonstrated the ability to generate high Reynolds number shear flow in water with angular momentum flux comparable to viscous transport (a null result in trying to demonstrate subcritical hydrodynamic instability [16]). The volume between the concentric rotating cylinders is filled with GaInSn, a gallium eutectic alloy [17]. The dimensions of the experiment and properties of the liquid metal are given in Table I.

The equations describing the evolution of a rotating shear flow with a background magnetic field are given by the magnetohydrodynamic (MHD) equations in a rotating frame:

$$\frac{\partial \mathbf{v}}{\partial t} + (\mathbf{v} \cdot \nabla) \mathbf{v} + 2\boldsymbol{\Omega} \times \mathbf{v} = -\nabla P + \frac{1}{\mu_0 \rho} (\mathbf{B} \cdot \nabla) \mathbf{B} + \nu \nabla^2 \mathbf{v}$$

$$\frac{\partial \mathbf{B}}{\partial t} = \nabla \times (\mathbf{v} \times \mathbf{B}) + \eta \nabla^2 \mathbf{B} \quad P = \frac{p}{\rho} + \frac{1}{2} \frac{B^2}{\mu_0 \rho} - \frac{1}{2} |\boldsymbol{\Omega} \times \mathbf{r}|^2$$

where \mathbf{v} and \mathbf{B} are solenoidal fields representing the velocity and magnetic field, $\boldsymbol{\Omega}$ is the angular velocity, and p is the pressure. The generalized pressure P incorporates the magnetic and centrifugal pressure terms.

The background field and angular velocity are given by $\mathbf{B}_0 = B_0 \hat{\mathbf{z}}$ and $\boldsymbol{\Omega} = \Omega \hat{\mathbf{z}}$. If we assume harmonic perturbations of the velocity and magnetic field and linearize the resulting equations, we obtain the dispersion relation in cylindrical coordinates [18]:

TABLE I. Physical parameters of the apparatus [15] and liquid metal [17].

Experimental parameters	Symbol	Units	Value
Height	h	cm	27.9
Inner cylinder radius	r_1	cm	7.06
Outer cylinder radius	r_2	cm	20.30
Density	ρ	g/cm ³	6.36
Kinematic viscosity	ν	cm ² /s	2.98×10^{-3}
Magnetic diffusivity	η	cm ² /s	2.57×10^3

$$\begin{aligned}
& (\bar{\omega} - i\gamma_\eta)^2 [(\bar{\omega} - i\gamma_\nu)(\bar{\omega} - i\gamma_\eta) + \omega_A^2]^2 \\
& + 2\zeta\Omega^2(\bar{\omega} - i\gamma_\eta)^4(k_z/k)^2 \\
& - 2(2 - \zeta)\Omega^2\omega_A^2(\bar{\omega} - i\gamma_\eta)(k_z/k)^2 \\
& - \omega_R [(\bar{\omega} - i\gamma_\nu)(\bar{\omega} - i\gamma_\eta) + \omega_A^2][(\bar{\omega} - i\gamma_\eta)^2 + \omega_A^2] = 0,
\end{aligned} \tag{1}$$

where $k_\phi = m/r$ for integer m , $\bar{\omega} = \omega - m\Omega$ is the Doppler-shifted complex frequency, $\gamma_\eta = \eta k^2$ and $\gamma_\nu = \nu k^2$ are the resistive and viscous damping rates, $\omega_A = k_z B_0 / \sqrt{\mu_0 \rho}$ is the Alfvén frequency, and $\omega_R = (\zeta - 2)\Omega k_r k_\phi / k^2$ is the Rossby wave frequency [19]. We have quantified the flow shear by introducing the vorticity parameter

$$\zeta(r) = \hat{\mathbf{z}} \cdot \frac{\nabla \times r\Omega(r)\hat{\phi}}{\Omega(r)} = \frac{1}{r\Omega} \frac{\partial(r^2\Omega)}{\partial r}. \tag{2}$$

Note that ζ is only constant if the rotation profile follows a power-law dependence $\Omega(r) \propto r^{\zeta-2}$. For uniform rotation with no shear $\zeta = 2$. The Rayleigh criterion [20], which governs axisymmetric hydrodynamic centrifugal stability of rotating shear flow, is given by $\zeta \geq 0$.

We can gain insight into the basic waves for this dispersion relation by examining limiting cases. In the absence of rotation, the dispersion relation reduces to

$$(\omega - i\gamma_\nu)(\omega - i\gamma_\eta) - \omega_A^2 = 0, \tag{3}$$

which describes the damped shear Alfvén wave. These waves have a transverse polarization due to the incompressibility of the fluid (in a compressible fluid there is also a longitudinal magnetosonic wave). The complex frequency is $\omega = i(\gamma_\nu + \gamma_\eta)/2 \pm \sqrt{\omega_A^2 - (\gamma_\nu - \gamma_\eta)^2}$ which shows that the Alfvén wave is viscously and resistively damped and has a real frequency of $\pm\omega_A$ in the absence of dissipation. Variations in the flow along the direction of the magnetic field tend to be eliminated in a highly resistive fluid (such as a liquid metal) due to this damping.

Assuming rotation without shear and without an applied magnetic field, the dispersion relation reduces to

$$(\omega - i\gamma_\nu)^2 + (2\Omega k_z/k)^2 = 0 \tag{4}$$

which describes inertial waves. Inertial waves also have a transverse polarization but are peculiar in that the restoring force, provided by the Coriolis effect, acts orthogonally to the displacement. The resulting motion of a displaced fluid element is circular precession. The complex frequency is $\omega = i\gamma_\nu \pm 2\Omega k_z/k$ so the wave is viscously damped with a real frequency between $\pm 2\Omega$. Note that there is no dependence on the wavelength. Akin to Alfvén waves, inertial waves homogenize the flow along the axis of rotation due to viscous damping, consistent with the Taylor-Proudman theorem [4].

Together these waves make up the hybrid magnetocoriolis wave [3]. Since there are two restoring forces acting on

displaced fluid elements, there are two possible situations. The Lorentz and Coriolis forces may act together, stiffening the system and producing the higher frequency fast wave, or the two forces may oppose one another to produce the lower frequency slow wave. The requirement for observing strong rotational effects on the Alfvén wave is $r\Omega\sqrt{\mu_0\rho}/B_0 \sim 1$. The Alfvén frequency experiences a splitting due to the breaking of the degeneracy of the two roots by the presence of rotation. When the flow has sufficient shear, the slow MC wave becomes stationary and unstable at low k as seen in Fig. 1. This instability is the MRI which in addition to causing turbulent transport of angular momentum in accretion disks may also be related to geomagnetic jerks [21].

The results reported here were obtained when an axial magnetic field was applied to turbulent rotating shear flow. The outer cylinder was kept stationary while the inner cylinder rotated. The rings at the end caps were coupled to either cylinder in what is referred to as the “split” configuration [15]. The flow was hydrodynamically unstable since $\zeta \leq 0$. The inner cylinder and inner ring

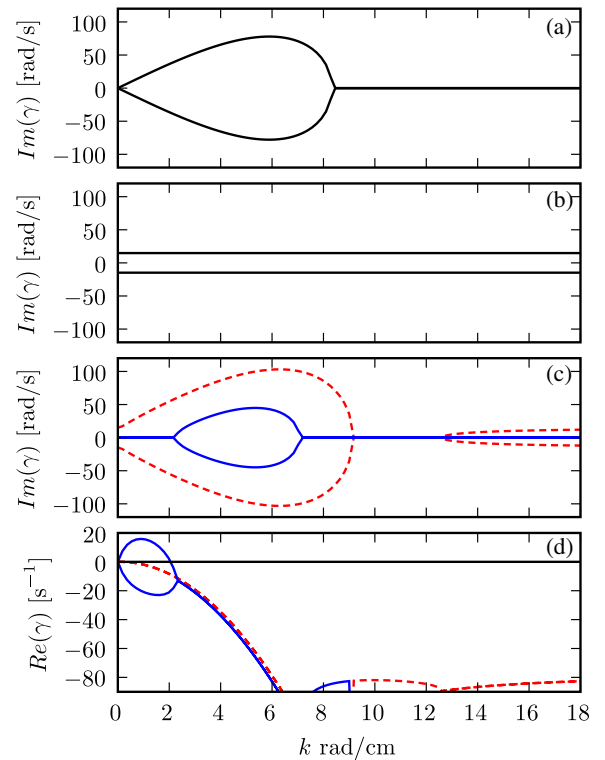


FIG. 1 (color online). The real part of the dispersion relation for (a) damped Alfvén waves as given in Eq. (3), (b) inertial waves as given in Eq. (4), and (c) the fast (dashed red line) and slow MC waves (solid blue line). (d) The growth rate of the fast and slow MC waves. Because of resistive dissipation, the MC waves collapse to the inertial wave dispersion at high k . When there is sufficient flow shear, the slow MC wave becomes unstable at low k . The parameters for the dispersion relation are $B_0 = 4$ kG, $\Omega = 42$ rad/s, and $\zeta = 0.25$ (maximum design parameters of the apparatus) and the fluid properties are given in Table I.

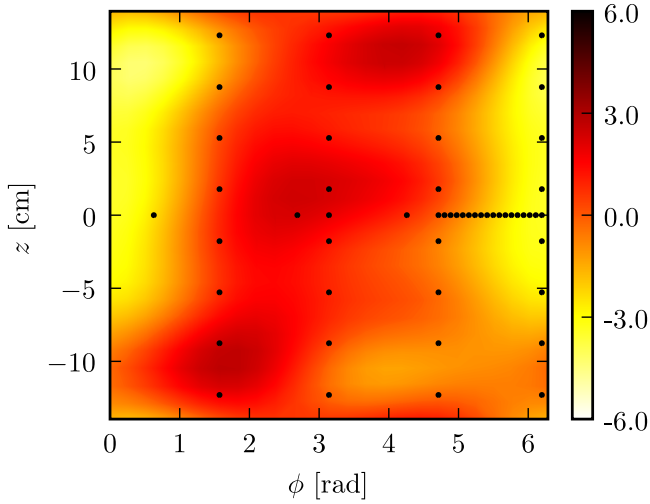


FIG. 2 (color online). A contour plot of the radial magnetic field near the surface of the outer cylinder constructed from a least squares fit of data from the Mirnov coil array. The locations of the coils are depicted by dots and the contour levels are given in Gauss. The applied field was 4.3 kG.

were set in rotation at 6.7 Hz and an axial magnetic field between 1.7 to 4.3 kG was applied to the turbulent flow. The induced radial magnetic field fluctuations were measured by an array of Mirnov coils [22] positioned just outside the outer cylinder. A nonaxisymmetric mode was apparent from the coil array as seen in the snapshot of the field shown in Fig. 2. The image is created by fitting the signals from the array to a spatial Fourier mode model using standard least squares fitting. From the model we obtain the Fourier amplitude and phase as shown in Fig. 3. The variation of the mode amplitudes with magnetic field strength is not linear as would be expected for advection by differential rotation (the Ω effect).

The mode rotation rates are measured by calculating the linear slope of the Fourier phase with time for each field strength. The results are shown in Fig. 4. The modes clearly rotate at different speeds and their rotation rates increase with magnetic field strength. By comparing the rotation

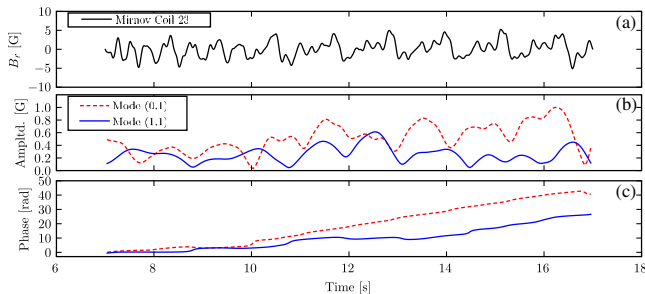


FIG. 3 (color online). (a) Magnetic field measured by a single Mirnov coil. (b) The time series of (0,1) and (1,1) mode amplitudes from a 2D Fourier decomposition of the radial magnetic field where the notation (n, m) describes the vertical mode number n and the azimuthal mode number m . (c) The time series of mode phases.

rates with those of higher azimuthal harmonics obtained from the high density midplane coil array (seen as the series of dots at $z = 0$ in Fig. 2) we find that the harmonics are not phase locked. Hence, the signal is not likely due to a passing vortex as was observed in Sisan *et al.* [11]. They are also not the result of the MRI since the least-damped mode should be axisymmetric.

A least squares fit of the observed mode rotation rates to the real frequencies of the fast and slow MC waves gives an estimate of the local wave vector components and the fluid rotation rate for a given shear. The wave number components are fit since the observed magnetic field is much smoother than the velocity field due to the low Pm and cannot reveal detailed structures like the boundary layers. The fit is insensitive to the vorticity parameter ζ and so we assume it to be zero for marginal stability consistent with hydrodynamic observations [23]. The fit parameters result in a mode with $k_z = \pi/2h$ and $k_r = \pi/(r_2 - r_1)$ which corresponds to the smallest (and therefore least-damped) radial wave number that can fit in the radial gap and a quarter-wavelength vertically. The growth rate determined from the fit is shown in Fig. 4(b). Aside from an expected Doppler shift for the nonaxisymmetric modes, the MC-wave model provides an excellent fit to the observations. From the growth rate, we find that the slow wave has a small positive growth rate for 1 kG but is otherwise damped. The model suggests that the MRI growth rate is too small at the rotation rates achieved to observe it with our diagnostics. By adjusting the model parameters we can

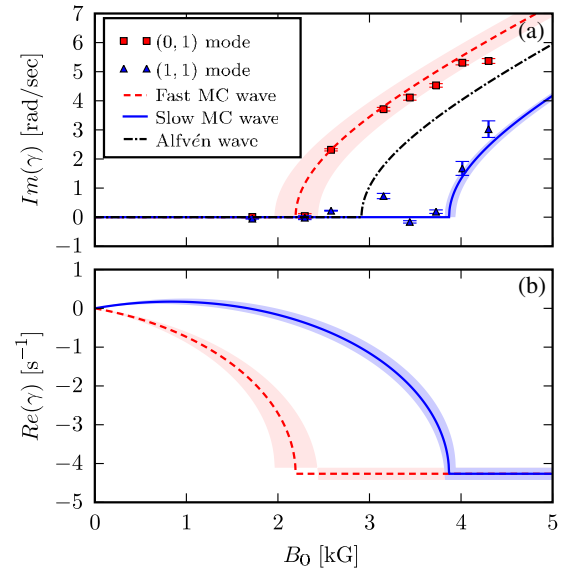


FIG. 4 (color online). The real frequency (a) and growth rate (b) determined by fitting the phase speed of the two nonaxisymmetric modes observed for a range of applied magnetic field strengths to Eq. (1). Error bars reflect the uncertainty in the linear fit to the phase as a function of time. The dashed red and solid blue lines show the fit of the fast and slow MC waves from Eq. (1) with values of $\zeta = 0$, $k = 0.246 \pm 0.001 \text{ cm}^{-1}$, $\theta = 1.336 \pm 0.007 \text{ rad}$ where $k_z = k \cos \theta$, and $\Omega = 5.4 \pm 0.9 \text{ rad/s}$. The shaded areas express the uncertainty in the fit.

predict the necessary rotation rate and magnetic field strength to observe the MRI based on the empirical observations of damped waves.

Nonaxisymmetric waves have been observed in the PROMISE magnetized Taylor-Couette experiment [24] which has also observed the helical MRI [10,25]. Sisan *et al.* [26] also observed rotating nonaxisymmetric spherical harmonic patterns in a turbulent liquid sodium spherical Couette flow which they attribute to the MRI, but may be due to a shear instability of the secondary meridional flow [27]. Runout of the inner cylinder could lead to a spinover mode due to the elliptical instability, but it is suppressed by the magnetic field [28]. It is still unclear why these nonaxisymmetric waves are favored over the axisymmetric ones, and its resolution may require 3D simulations as well as internal flow and magnetic field measurements.

One conjecture regarding the source of these damped waves is that the turbulent flow provides perturbations of a broad range of wavelengths, but that the geometry of the vessel dictates which modes are realized [29]. Such is observed when a precessing top cap is used to drive inertial waves in a cylinder filled with water [30]. The observed waves in this case are cavity resonances driven by unstable flow at the boundary discontinuities and not an instability of the bulk flow. It is also possible that these damped waves are driven through nonlinear wave coupling [31]. If such is the case, then these damped waves may be a saturation mechanism for the MRI. Although we have not observed the MRI in the experiment, nonlinear simulations of single mode MRI found that saturation was achieved by amplifying the vertical field through an α effect [32]. It is due to the ambiguity of the source of these waves that we are continuing to pursue an observation of magnetically induced instability in a hydrodynamically quiescent flow.

In summary, we have observed rotating modes in a turbulent Taylor-Couette flow of liquid metal that we identify as the fast and slow MC wave. We have identified a relationship between the slow MC wave and the MRI and have proposed a method of determining the threshold for instability through observation of driven MC waves. MC waves will be important in identifying the MRI in further experiments and may also play a role in saturation of MHD turbulence in rotating fluids.

We thank Chris Finlay for helpful discussions and pointing out valuable references and Hans Rinderknecht for his contributions on dispersion relation calculations as a senior project of Princeton University. This work was funded under NASA Grants No. ATP03-0084-0106 and No. APRA04-0000-0152, DOE Contract No. DE-AC02-09CH11466, and NSF Grant No. AST0607472.

*Present address: Department of Physics at the University of Wisconsin-Madison, 1150 University Ave., Madison, WI 53706, USA.

- [1] S. Lundquist, *Phys. Rev.* **76**, 1805 (1949).
- [2] H. Alfvén, *Nature (London)* **150**, 405 (1942).
- [3] D. Acheson and R. Hide, *Rep. Prog. Phys.* **36**, 159 (1973).
- [4] H. Greenspan, *The Theory of Rotating Fluids* (Cambridge University Press, Cambridge, U.K., 1968).
- [5] R. Hide, *Phil. Trans. R. Soc. A* **259**, 615 (1966).
- [6] P. Kumar, S. Talon, and J.-P. Zahn, *Astrophys. J.* **520**, 859 (1999).
- [7] P. H. Roberts and A. M. Soward, *Annu. Rev. Fluid Mech.* **4**, 117 (1972).
- [8] C. C. Finlay, in *Dynamos*, Lecture Notes of the Les Houches Summer School Vol. LXXXVIII, edited by P. Cardin and L. Cugliandolo (Elsevier, New York, 2008), Chap. 8.
- [9] S. A. Balbus and J. F. Hawley, *Astrophys. J.* **376**, 214 (1991).
- [10] F. Stefani, T. Gundrum, G. Gerbeth, G. Rüdiger, M. Schultz, J. Szklarski, and R. Hollerbach, *Phys. Rev. Lett.* **97**, 184502 (2006).
- [11] D. R. Sisan, W. L. Shew, and D. P. Lathrop, *Phys. Earth Planet. Inter.* **135**, 137 (2003).
- [12] D. Schmitt, T. Alboussière, D. Brito, P. Cardin, N. Gagnière, D. Jault, and H. Nataf, *J. Fluid Mech.* **604**, 175 (2008).
- [13] E. J. Spence and K. Reuter, *Bull. Am. Phys. Soc.* **53**, 299 (2008).
- [14] D. H. Kelley, S. A. Triana, D. S. Zimmerman, A. Tilgner, and D. P. Lathrop, *Geophys. Astrophys. Fluid Dyn.* **101**, 469 (2007).
- [15] E. Schartman, H. Ji, and M. J. Burin, *Rev. Sci. Instrum.* **80**, 024501 (2009).
- [16] H. Ji, M. Burin, E. Schartman, and J. Goodman, *Nature (London)* **444**, 343 (2006).
- [17] N. B. Morley, J. Burris, L. C. Cadwallader, and M. D. Nornberg, *Rev. Sci. Instrum.* **79**, 056107 (2008).
- [18] H. Ji, J. Goodman, and A. Kageyama, *Mon. Not. R. Astron. Soc.* **325**, L1 (2001).
- [19] C. Rossby *et al.*, *J. Mar. Res.* **2**, 38 (1939).
- [20] L. Rayleigh, *Proc. R. Soc. A* **93**, 148 (1917).
- [21] L. Petitdemange, E. Dormy, and S. Balbus, *Geophys. Res. Lett.* **35**, L15305 (2008).
- [22] I. Hutchinson, *Principles of Plasma Diagnostics* (Cambridge University Press, Cambridge, U.K., 2002).
- [23] G. S. Lewis and H. L. Swinney, *Phys. Rev. E* **59**, 5457 (1999).
- [24] F. Stefani, T. Gundrum, G. Gerbeth, G. u. Rüdiger, J. Szklarski, and R. Hollerbach, *New J. Phys.* **9**, 295 (2007).
- [25] G. Rüdiger, R. Hollerbach, F. Stefani, T. Gundrum, G. Gerbeth, and R. Rosner, *Astrophys. J.* **649**, L145 (2006).
- [26] D. Sisan, N. Mujica, W. Tillotson, Y. Huang, W. Dorland, A. Hassam, T. Antonsen, and D. Lathrop, *Phys. Rev. Lett.* **93**, 114502 (2004).
- [27] R. Hollerbach, *Proc. R. Soc. A* **465**, 2003 (2009).
- [28] W. Herreman, M. Le Bars, and P. Le Gal, *Phys. Fluids* **21**, 046602 (2009).
- [29] W. Wood, *J. Fluid Mech.* **22**, 337 (1965).
- [30] A. McEwan, *J. Fluid Mech.* **40**, 603 (1970).
- [31] P. W. Terry, *Phys. Rev. Lett.* **93**, 235004 (2004).
- [32] F. Ebrahimi, S. C. Prager, and D. D. Schnack, *Astrophys. J.* **698**, 233 (2009).